



Effects of Wall-Ash and Plug-Ash on Pressure Drop and Soot Deposition in Diesel Particulate Filter

Kazuhiro Yamamoto¹ · Takuya Morimoto¹

Received: 26 May 2022 / Revised: 20 July 2022 / Accepted: 22 August 2022 / Published online: 6 September 2022
© The Author(s), under exclusive licence to Springer Nature Switzerland AG 2022

Abstract

Currently, a diesel particulate filter (DPF) is used to trap particulate matters (PMs) of diesel soot. Since the pressure drop during the PM filtration, a filter regeneration is needed for soot oxidation. However, PM includes incombustible substances originated from the engine lubricant oil additives, and ash remains after the regeneration. There are two types of ash, wall-ash and plug-ash. In this study, by changing the ratio of wall-ash and plug-ash, we have simulated the flow and the soot filtration of DPF with different ash layer distributions. The single channel of the DPF was considered, by using the wall substrate structure scanned by the X-ray CT. When the initial pressure drop before the soot deposition is divided into four contributions at the DPF inlet, across the filter wall, at the DPF outlet, and in the channel due to the friction loss, the pressure drop across the filter wall is the largest, accounting for more than 86% of the total pressure drop. The initial pressure drop increases at higher ratio of the wall-ash. In the case of no ash or plug-ash only, the transition of the depth filtration to the surface filtration is observed. On the other hand, when the DPF wall is fully covered with ash, only the surface filtration occurs, which suppresses an increase in the pressure drop. Overall, the wall-ash largely reduces the pressure drop by avoiding the depth filtration, but the thicker wall-ash layer increases the pressure drop on the condition that the total amount of the wall-ash and the plug-ash is the same.

Keywords Filtration · DPF · Ash · Pressure drop · Simulation

1 Introduction

To remove diesel soot in exhaust gas, named particulate matter (PM), a well-known diesel particulate filter (DPF) is used in the after-treatment system [1–7]. It is a wall-flow filter, which consists of cells with inlet and outlet channels separated by porous filter walls. For reducing NO_x, a selective catalytic reduction (SCR) system is also used. Ximinis et al. have investigated the suitable placements of DPF and SCR to increase the efficiency of the catalytic reaction [8]. It is important to optimize the DPF and SCR placement, because the DPF/DOC degradation may allow particles to pass downstream to the SCR, resulting in the reduction of the SCR catalytic activity. In recent years, stricter PM regulations on gasoline exhaust emissions have necessitated the

use of gasoline particulate filters (GPFs) as well [9–12], because higher particle emissions from spark-ignition direct-injection (SIDI) engines have been reported [13].

However, PM-loaded DPF increases the pressure drop due to agglomeration of deposited particles, causing engine performance degradation and fuel consumption deterioration [14–18]. Therefore, the DPF regeneration process is necessary to burn out (oxidize) the deposited soot particles [1, 2, 7]. As for the DPF regeneration, there are so-called active and passive types [19, 20]. As for the active regeneration, it is initiated by the post-fuel injection in the engine's cylinders during the late expansion stroke or directly in the exhaust line so that the exhaust gas temperature is increased by the diesel oxidation catalyst (DOC) [21]. The approximate temperature for the active regeneration is about 500 to 550 °C [22, 23]. Frequent of active regeneration events cause the extra fuel consumption. As for the passive regeneration, the temperature at which soot is oxidized by NO₂ is about 260 to 320 °C [24]. Nevertheless, since PM includes incombustible substances, ash remains after the regeneration, typically composing of calcium, zinc, and magnesium

✉ Kazuhiro Yamamoto
kazuhiro@mech.nagoya-u.ac.jp

¹ Department of Mechanical System Engineering,
Nagoya University, Furo-cho, Chikusa-ku, Nagoya-shi,
Aichi 464-8603, Japan

compounds in the form of various metallic oxides, sulfates, and phosphates. It is reported that more than 90% of the ash in the DPF originates from the engine lubricant oil additives [25]. It should be noted that there are two types of ash: wall-ash, which is deposited in a layer on the inlet channel surfaces of the filter wall of the DPF, and plug-ash, which plugs at the outlet of the DPF [26–28]. Resultantly, the pressure drop cannot recover to the level of the clean filter even after the regeneration, and the regeneration needs to be more frequent, reducing the service life of the DPF [20].

So far, many fundamental researches have been conducted. For example, Zhang et al. have investigated the effect of the ash on the active regeneration of the DPF using the engine test bench [25]. Aravelli et al. [26] have found that in some cases the ash will reduce the high pressure drop associated with depth filtration of soot into the substrate during the soot filtration, corresponding to a membrane effect. Sappok et al. have investigated the effects of the ash composition, reporting that the pressure drop is a function of the ash chemistry due to the ash particles have differing particle size, packing characteristics, particle morphology, and ultimately permeability [27, 28]. Ishizawa et al. have investigated the effect of the temperature during regeneration on the ash deposition and its composition [29]. Jiang et al. have proposed a mathematical model of ash and clarified the effects of the ash on the filtration efficiency of the DPF [30]. Fang et al. have investigated the size and the composition of deposited ash during the DPF regeneration process [31]. Lao et al. have conducted a numerical study of thermal treatment of the filter with plug-ash [32]. In some simulations [22, 33–35], the filter wall has been assumed to be uniform media. To evaluate the pressure drop with soot deposition, the substrate wall permeability is set. In this case, a model parameter is needed to consider the transition of the depth filtration to the surface filtration [36]. However, at the earlier stage of the soot filtration, soot is deposited inside the non-uniform filter wall, which causes the large pressure drop [37]. However, the ash prevents the depth filtration in the DPF pores, resulting in the smaller pressure drop [38]. Thus, to reproduce the depth filtration, we must consider the flow and soot deposition inside the filter wall with complex substrate structure. Few studies have systematically examined how wall-ash and plug-ash separately affect the soot deposition process and the pressure drop. For this purpose, it is desirable to investigate the soot deposition behavior and the pressure drop of the DPF with the ash layer by the numerical simulation.

In our previous studies, we have used the lattice Boltzmann method (LBM) to simulate the flow and the soot deposition in the DPF [6, 37, 39–44]. Our approach is the numerical simulation coupled with an X-ray CT measurement for

scanning the substrate structure of the DPF, which is called a tomography-assisted simulation. Then, the flow field in the real ceramic filter can be produced to examine the filtration process in detail. However, in our simulation, only a part of the filter wall has been considered, because the image size of the X-ray CT measurement is limited. In this study, a new trial was tested to construct the single channel by using the DPF wall of the X-ray CT substrate structure. The original substrate structure of the DPF wall without ash was referred to case 1. Additionally, five cases were considered, in which ash was deposited by changing the ratio of the wall-ash and the plug-ash. By comparing the numerical simulations in these six cases, we tried to clarify how the wall-ash and the plug-ash could affect the flow and the soot deposition process, based on the change in the pressure drop due to the ash layer distribution.

2 Model Description

2.1 Governing Equations and Filtration Model

For simulation of flow with soot deposition in the DPF, we have used a lattice Boltzmann method (LBM), which is suitable for the porous media flow [45]. Here, the approach and the equations are explained. To conduct the 3D simulation, a D3Q15 model [46] was applied. In this velocity model, 15 discrete velocities in the lattice space are used, which are described by

$$\begin{bmatrix} c_1 & c_2 & c_3 & c_4 & c_5 & c_6 & c_7 & c_8 & c_9 & c_{10} & c_{11} & c_{12} & c_{13} & c_{14} & c_{15} \\ 1 & -1 & 0 & 0 & 0 & 0 & 1 & -1 & 1 & -1 & 1 & -1 & 1 & -1 & 0 \\ 0 & 0 & 1 & -1 & 0 & 0 & 1 & -1 & 1 & -1 & -1 & 1 & -1 & 1 & 0 \\ 0 & 0 & 0 & 0 & 1 & -1 & 1 & -1 & -1 & 1 & 1 & -1 & -1 & 1 & 0 \end{bmatrix} \quad (1)$$

where c_α ($\alpha=1$ to 15) is the advection velocity in the lattice space. The evolution equation for the flow is

$$p_\alpha(\mathbf{x} + \mathbf{c}_\alpha \delta_t, t + \delta_t) - p_\alpha(\mathbf{x}, t) = -\frac{1}{\tau_p} [p_\alpha(\mathbf{x}, t) - p_\alpha^{eq}(\mathbf{x}, t)] - \frac{\tau_p - 0.5}{\tau_p} F_i \quad (2)$$

where δ_t is the time step, τ_p is the relaxation time to the equilibrium distribution caused by the molecular collision in the flow, and F_i is the external force term (see Eq. (7)). The kinetic viscosity is expressed by the formula of $\nu = (2\tau_p - 1)/6 c^2 \delta_t$. The equilibrium distribution function of p_α^{eq} is

$$p_\alpha^{eq} = w_\alpha \left\{ p + p_0 \left[3 \frac{(\mathbf{c}_\alpha \cdot \mathbf{u})}{c^2} + \frac{9}{2} \frac{(\mathbf{c}_\alpha \cdot \mathbf{u})^2}{c^4} - \frac{3}{2} \frac{\mathbf{u} \cdot \mathbf{u}}{c^2} \right] \right\} \quad (3)$$

where $w_\alpha = 1/9$ ($\alpha = 1:6$), $w_\alpha = 1/72$ ($\alpha = 7:14$), and $w_{15} = 2/9$. The sound speed, c_s , is $c/\sqrt{3}$ with the ideal gas equation of $p_0 = \rho_0 RT_0 = \rho_0 c_s^2$, where p_0 and ρ_0 are the pressure and the density at the reference temperature (room temperature). In this simulation, only the soot filtration is simulated with the constant temperature of the exhaust gas. The pressure and the flow velocity of $\mathbf{u} = (u_x, u_y, u_z)$ are evaluated in terms of the low Mach number approximation [47]. All variables of the flow are obtained by the LBM, by considering the similarity of the Reynolds number of $Re = U_{in}W/\nu$ and the Mach number of $Ma = U_{in}/c_s$. Here, U_{in} is the inflow velocity of the exhaust gas at the inlet and W is the thickness of the filter wall. The pressure and the local velocity are obtained by

$$p = \sum_{\alpha} p_{\alpha} \tag{4}$$

$$\mathbf{u} = \frac{\rho_0}{\rho} \frac{\sum_{\alpha} \mathbf{c}_{\alpha} p_{\alpha}}{p_0} + 0.5f\delta_t \tag{5}$$

$$\mathbf{f} = -\frac{\nu}{\kappa} \mathbf{u} \tag{6}$$

$$F_i = \frac{-3\mathbf{f} \cdot (\mathbf{e}_{\alpha} - \mathbf{u})}{c^2} f_{\alpha}^{eq} \tag{7}$$

where r is the density of the exhaust gas, \mathbf{f} is the external force, and κ is the permeability. It is known that the permeability of the soot layer depends on the flow of the exhaust gas that passes through the filter wall, the diameter of the primary soot particles, and the diffusion coefficient of aggregate soot particles. In the simulation, based on the Peclet number (Pe) of the soot deposited by the filter [48], the permeability is given.

On the other hand, the mass fraction of soot is obtained by solving the following distribution function of soot.

$$f_{c,\alpha}(\mathbf{x} + \mathbf{c}_{\alpha}\delta_t, t + \delta_t) - f_{c,\alpha}(\mathbf{x}, t) = -\frac{1}{\tau_c} [f_{c,\alpha}(\mathbf{x}, t) - f_{c,\alpha}^{eq}(\mathbf{x}, t)] \tag{8}$$

$$f_{c,\alpha}^{eq}(\mathbf{x}, t) = w_{\alpha} Y_c \left\{ 1 + 3\left(\frac{\mathbf{c}_{\alpha} \cdot \mathbf{u}}{c^2}\right) + \frac{9}{2}\left(\frac{\mathbf{c}_{\alpha} \cdot \mathbf{u}}{c^2}\right)^2 - \frac{3}{2}\left(\frac{\mathbf{u}}{c}\right)^2 \right\} \tag{9}$$

As for the relaxation time τ_c , the same value of τ_p in Eq. (2) is used. The mass fraction of soot is calculated by

$$Y_c = \sum_{\alpha} f_{c,\alpha} \tag{10}$$

At the filter wall, the ash layer and the soot deposition region, the soot deposition occurs, which is calculated by

$$\rho_{soot}(\mathbf{x}, t + \delta_t) = \rho_{soot}(\mathbf{x}, t) + \rho \sum_{\alpha} f_{c,\alpha}(\mathbf{x}, t) \cdot \eta_{total} \tag{11}$$

where r_{soot} is the density of the soot deposition region and h_{total} is the total filtration efficiency. At the surface of the ash layer, the non-slip wall for the flow is set. Since the flow cannot pass through the soot layer, the soot is deposited only on the surface of the ash layer. It is noted that the soot which is not deposited is re-entrained to the original gas flow. Based on Eq. (11), the total density of the deposited soot region at the lattice node is calculated, and it reaches the threshold; this node is treated as the soot deposition layer. At the next time step, the soot deposition region is moved to one node next to the original boundary of the soot layer. In this way, the soot layer is thickened. The threshold is determined by the density of the soot layer, which is given by Pe [48]. As for the filtration efficiency, the Brownian diffusion and the interception effect are considered [36, 44], in which the total filtration efficiency is expressed by the filtration efficiency of the Brownian diffusion, h_D , and that of the interception effect, h_I , respectively.

$$\eta_I = 1.5 \times \{g(\epsilon_w)\}^3 \times \frac{\left(\frac{d_{soot}}{d_c}\right)^2}{\left(1 + \frac{d_{soot}}{d_c}\right)^{\frac{3-2\epsilon_w}{3\epsilon_w}}} \tag{12}$$

$$\eta_D = 3.5g(\epsilon_w)Pe^{-\frac{2}{3}} \tag{13}$$

$$g(\epsilon_w) = \sqrt[3]{\frac{\epsilon_w}{2 - \epsilon_w - \frac{9 \times \sqrt[3]{(1-\epsilon_w)}}{5} - \frac{(1-\epsilon_w)^2}{5}}} \tag{14}$$

$$\eta_{DI} = \eta_D + \eta_I - \eta_I \eta_D \tag{15}$$

$$\eta_{total} = 1 - \exp\left(-\frac{3\eta_{DI}(1 - \epsilon_w)W}{2\epsilon_w d_c}\right) \tag{16}$$

Here, g is a geometric coefficient, e_w is the porosity of the filter wall ($= 0.62$), and d_c is the mean particle diameter of the filter wall.

2.2 Substrate Structure and Numerical Conditions

As explained, the three-dimensional substrate structure of the DPF was obtained by the X-ray CT measurement. In this study, the wall-flow uncoated cordierite DPF was considered. The voxel size of this measurement was 1 μm . Figure 1 shows a part of the measured filter substrate structure. In the simulation, the soot filtration in the single channel of the DPF was examined, and the spatial grid size in the simulation must be as large as possible for the reduction of the computational costs. Therefore, using the original substrate

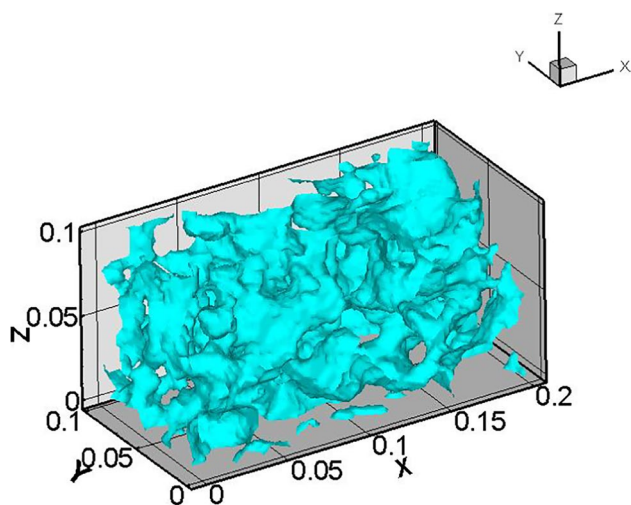


Fig. 1 Filter substrate measured by X-ray CT (unit is millimeter, mm)

structure with the CT resolution of 1 μm , we created several two-dimensional substrate structures with coarse resolution by the binarization. In the preliminary simulation, the dependence of the grid size was checked. The original substrate structure with the resolution of 1 μm is shown in Fig. 2a, together with the grid sizes of 2, 4, 8, and 16 μm prepared by ourselves in Fig. 2b–e. In the coordinate system, the direction in which the exhaust gas passes through the DPF wall is the y-axis (flow direction), and the direction perpendicular to the y-axis is the x-axis. After the spatial grid was finally determined, the whole numerical domain for the single channel of the DPF with density of 300 cps was produced, which is shown in Figs. 3 and 4.

Next, we explain the procedure for creating the DPF wall with the substrate structure by the X-ray CT. As shown in Fig. 3, we created the whole DPF wall by turning over and repeating the original substrate structure

Fig. 2 Numerical domain to investigate the spatial resolution with resolution of a 1 μm , b 2 μm , c 4, d 8 μm , e 16 μm

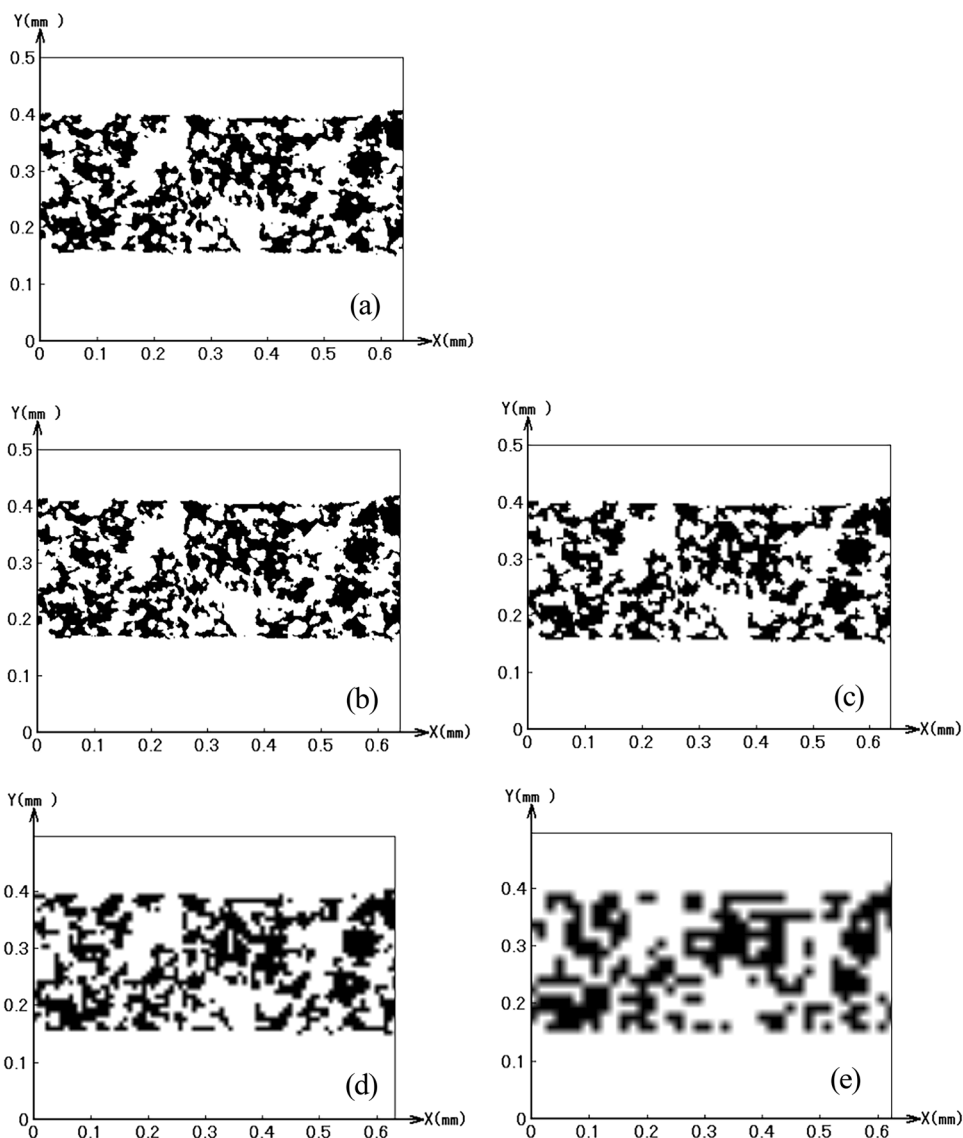


Fig. 3 Procedure for producing filter wall with the substrate structure of X-ray CT

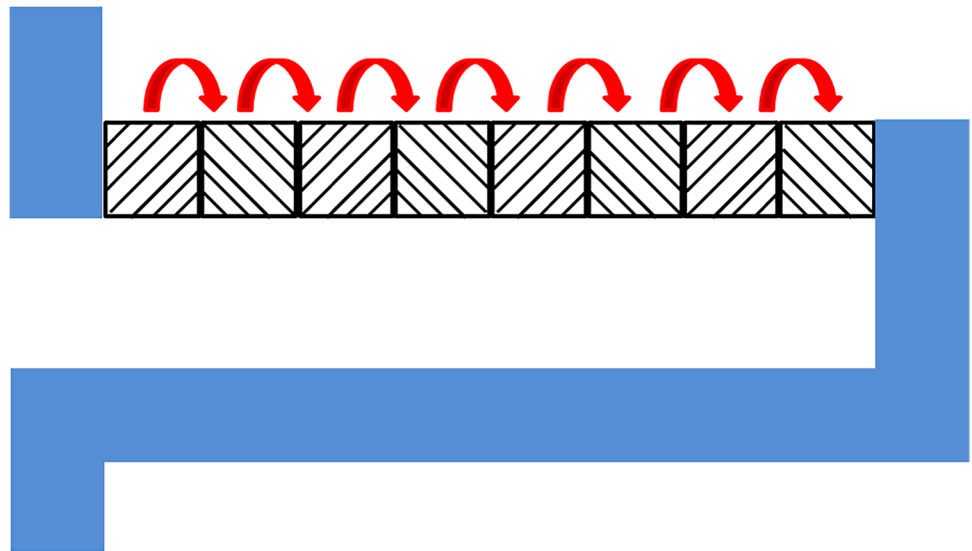
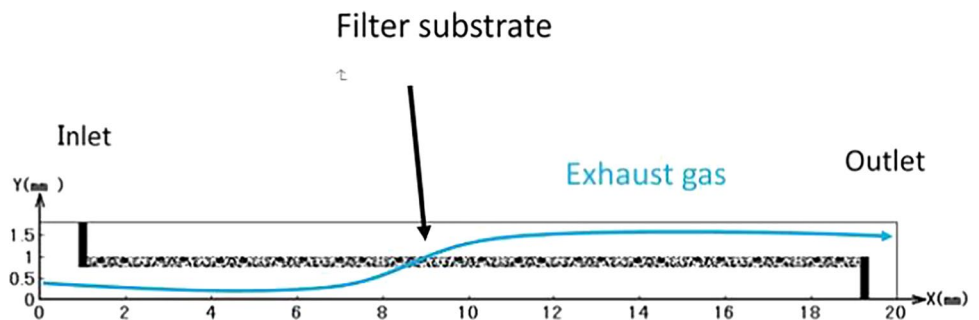


Fig. 4 Filter wall of the resolution of 4 μm in the numerical domain



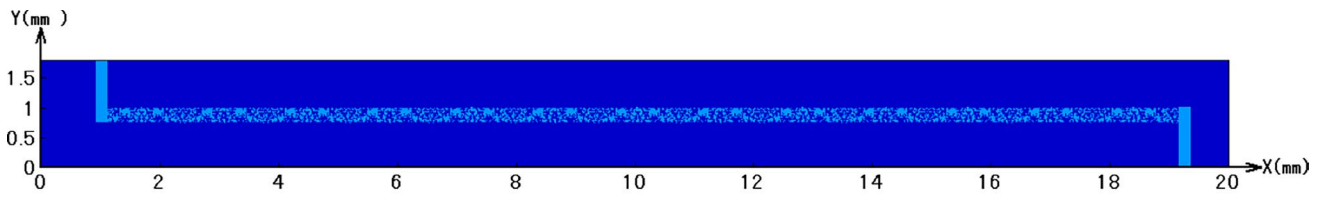
several times. The obtained two-dimensional substrate structure and the numerical domain are shown in Fig. 4. The front part of the DPF is located at $x = 1$ mm. The exhaust gas flow is roughly indicated by the arrow, and the size of the entire numerical domain is 20 mm (x) \times 1.8 mm (y). Numerical simulations were performed in six cases: case 1, without ash deposition layer, and cases 2 to 6, in which different ratios of the wall-ash and the plug-ash were placed by keeping the total amount of ash was $\rho_{\text{ash}} = 46.6$ g/L. It is noted that the total amount of ash is the ash amount divided by the filter volume [49], which is an important parameter for discussing the ash limit in the DPF. To calculate the total amount of ash in the present simulation, the ash packing density of 0.7 g/cm³ [33] is used. Figure 5 shows the location of the ash layer in the numerical domain, where the area of the yellow color is the ash layer. The thickness of the ash layer is constant along the wall, although realistic ash cake layers typically have a parabolic shape where the thickness increases from inlet to the top of the ash plug [49]. Table 1 shows the ratios of the wall-ash and the plug-ash. In this table, the initial pressure drops obtained by the steady flow before the soot deposition are shown.

Finally, the boundary conditions are described. The exhaust gas temperature was 423 K [4, 17]. As for the soot, the agglomerate particle size was 100 nm and its mass fraction in the exhaust gas flow was 0.1. At the inlet of the numerical domain which is located at $x = 0$ mm in front of the DPF, the inflow velocity was 43 cm/s. At the outlet passing through the rear end of the DPF, the pressure was kept constant at atmospheric pressure. At the upper or lower boundary of the numerical domain, a symmetrical boundary with a slip wall condition was adopted. On the other hand, a non-slip wall condition was applied at the surface of the filter substrate. The permeability of the soot deposition layer was set to be 2.0×10^{-14} m² referring to Ref. [50], and that of the ash layer was set to be 6.5×10^{-14} m² referring to Ref. [28]. The density of the soot deposition layer was 38 kg/m³.

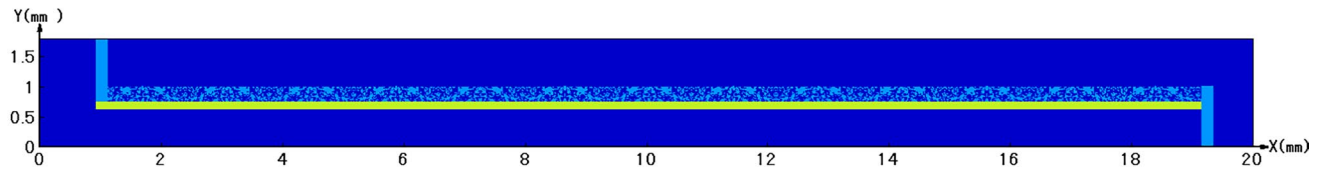
3 Results and Discussion

3.1 Flow Field Before Soot Deposition

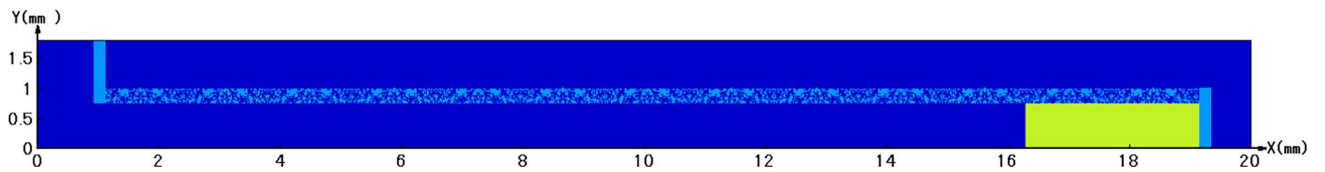
First, the flow before the soot deposition was simulated, where a steady flow field was obtained. It was to determine



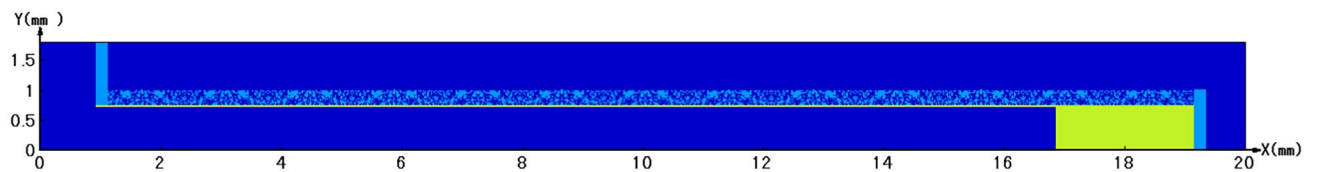
(a) Case 1



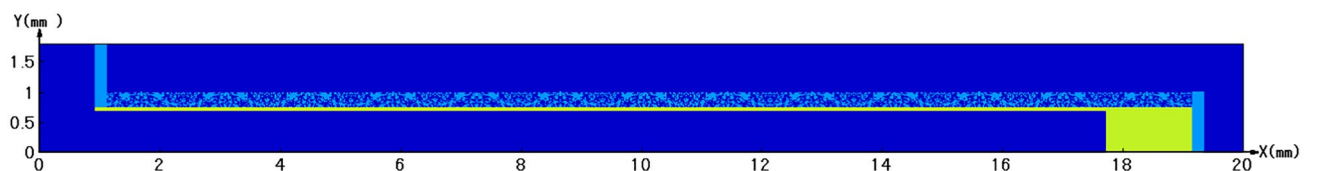
(b) Case 2



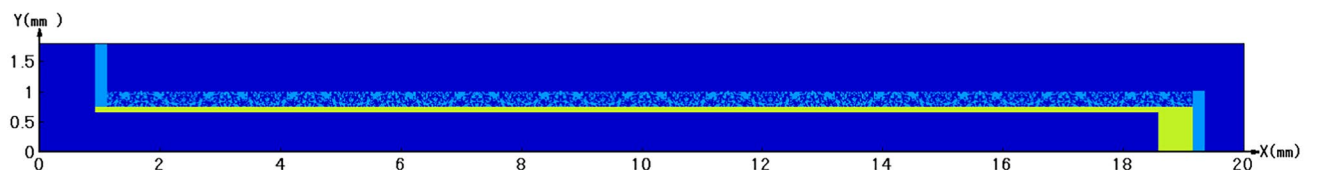
(c) Case 3



(d) Case 4



(e) Case 5

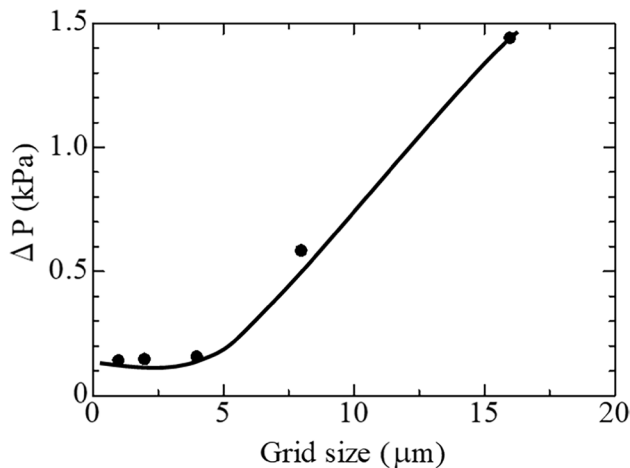


(f) Case 6

Fig. 5 Distributions of ash layer in the DPF for cases 1 to 6

Table 1 Fraction of wall-ash or plug-ash of the total amount of ash, with initial pressure drop

Case	Wall-ash (%)	Plug-ash (%)	ΔP_0 (kPa)
1	0	0	0.176
2	100	0	2.62
3	0	100	0.208
4	20	80	1.32
5	50	50	1.88
6	80	20	2.30

**Fig. 6** Initial pressure drop at different grid size

the appropriate grid size for the reduction of the computational costs as much as possible. The numerical domains of the preliminary simulation with five different grid sizes are shown in Fig. 2. Different from Fig. 4 of the single channel of the whole DPF wall simulation, the smaller numerical domain was considered by changing the grid size. As a result, it is found that the flow fields with grid sizes of 1, 2, and 4 μm are quite similar, but those of 8 and 16 μm show different flow patterns. This is because pores appearing in the porous filter wall are inevitably different due to the coarse spatial grid. To make clear the dependence of the spatial grid size, the initial pressure drop was examined, which is plotted in Fig. 6. It is found that the initial pressure drops of the grid size of 2 and 4 μm are almost the same as that of the original grid size of 1 μm of the X-ray CT measurement, and that those of 8 and 16 μm are very large. Resultantly, the grid size of 4 μm was used for further simulation of the single channel in Fig. 4.

Unfortunately, even in the two-dimensional simulation, a huge number of grid points would be required if the size of all grids was set to be 4 μm for the entire numerical domain. It should be noted that, different from the region of the porous filter wall, the larger grid size can be applied for the

gas phase where the flow and the pressure would not change much. Therefore, the grid size of 40 μm was used for the gas phase, which was 10 times larger than 4 μm , except for three regions of the inlet of the DPF, the DPF wall and the outlet of the DPF. Besides, the fine grid of 4 μm would be needed on the filter wall surface where the soot is expectedly deposited. For using two different spatial grids in the lattice Boltzmann simulation, it is necessary to interpolate the distribution function of the flow at the boundary of the numerical domain with the different grid size. Then, the interpolation LBM scheme proposed in ref. 47 was used to estimate the distribution function at coarse grids. To validate the simulation of the soot filtration by the interpolation LBM scheme, we compared the soot deposition profiles obtained by (1) the simulation of the combination of 4 μm and 40 μm spatial grids and (2) the simulation with the uniform grid of 4 μm . Since both soot deposition profiles were matched, we could confirm the validity of the present interpolation LBM scheme.

Next, we performed numerical simulations of the flow field with different ash layer in Table 1. The flow fields with velocity vectors in cases 1 to 6 are shown in Fig. 7, corresponding to the steady flows with different ash layer distributions. For better understanding the velocity field affected by the ash layer, the axial distributions of wall flow velocity in cases 1 to 6 are shown in Fig. 8. This is because the wall flow velocity is important during the soot filtration. These distributions are obtained at $y = 0.76$ mm, just before the filter wall. The flow field without ash is shown in Fig. 7a and b. It should be noted that, in the case of the wall-flow filter, the exhaust gas flows into the inlet channel, passes through the filter wall, and flows out from the outlet channel. At the inlet of the DPF of $x = 1$ mm, the flow changes largely because the flow is forced to enter the open channel [48]. After that, the flow parallel to the DPF wall is observed, a part of which passes through the filter wall and merges again. At the outlet of the DPF located roughly of $x = 19$ mm, the flow is slightly expanded. Based on the distribution of the wall flow velocity in Fig. 8a, it is found that the flow passes through some region preferentially, because there are limited paths across the filter wall. As seen in Fig. 7b, the similar flow field to that in Fig. 7a is observed in case 2 with wall-ash only. By comparing with Fig. 8a, the wall flow velocity in case 2 in Fig. 8b becomes relatively flat due to the wall-ash. Expectedly, different from case 1, the flows in cases 3 to 6 change due to the plug-ash. That is, the wall flow velocity is enlarged in Fig. 8c-f, because the effective filter volume is reduced due to the plug-ash [25, 32]. It is quite reasonable, because the flow tends to avoid the region of the plug-ash which imposes the large pressure drop.

Needless to say, the pressure drop must be changed when the flow is forced to pass through the ash layer, which may

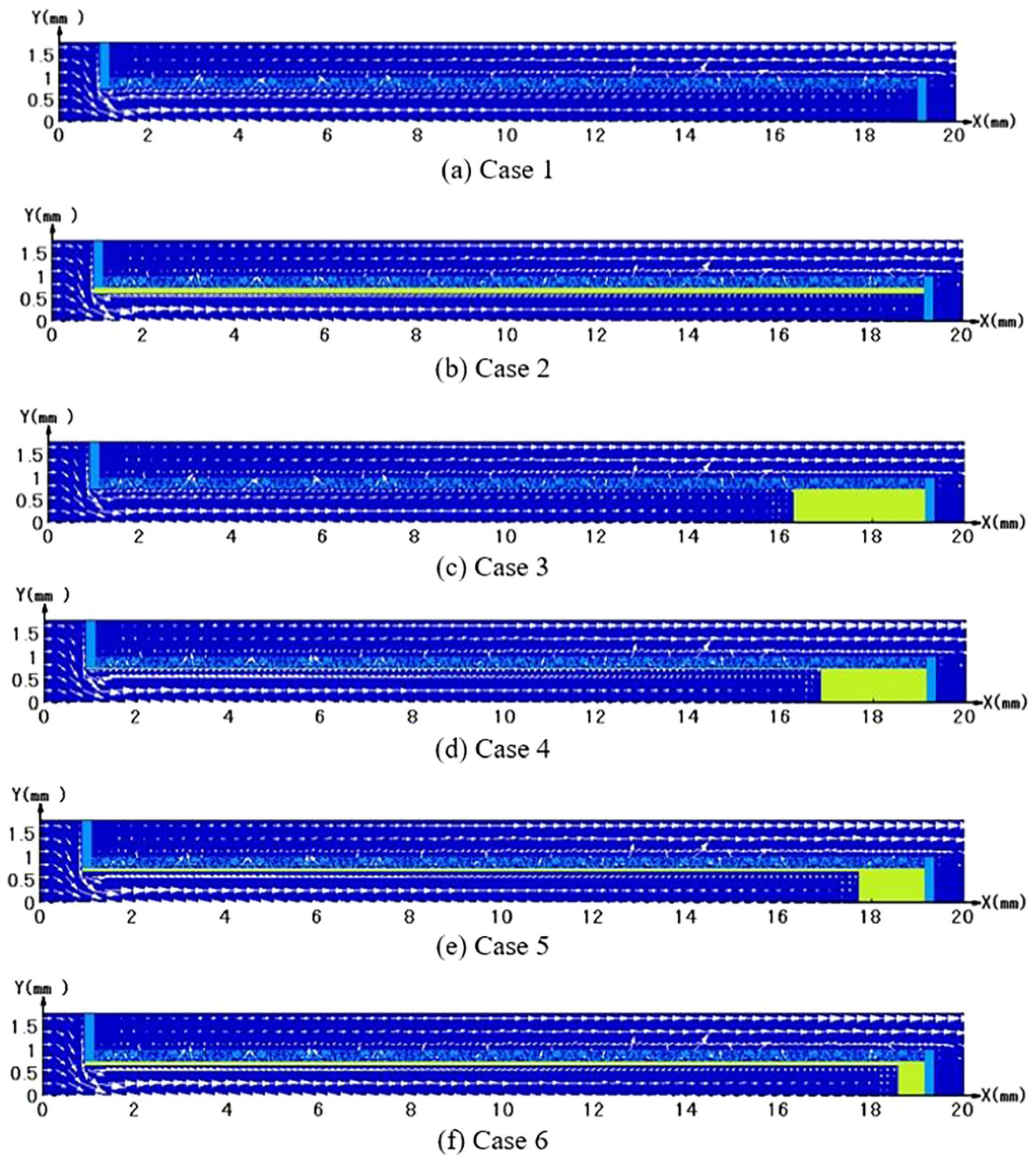


Fig. 7 Flow field with velocity vectors in cases 1 to 6

have a significant effect on the soot deposition process. The pressure drop before the soot deposition was examined. The initial pressure drops for conditions 1 to 6 are shown in Table 1. It is found that the pressure drop increases as the fraction of the wall-ash of the total amount of ash is higher.

In other words, compared with the plug-ash, the effect of the wall-ash on the initial pressure drop would be larger. For further investigation, we examined where the large pressure change was created. Then, the initial pressure drop in Table 1 was divided into four contributions: the pressure drop at the

Fig. 8 Axial distributions of wall flow velocity are shown; **a** case 1, **b** case 2, **c** case 3, **d** case 4, **e** case 5, **f** case 6

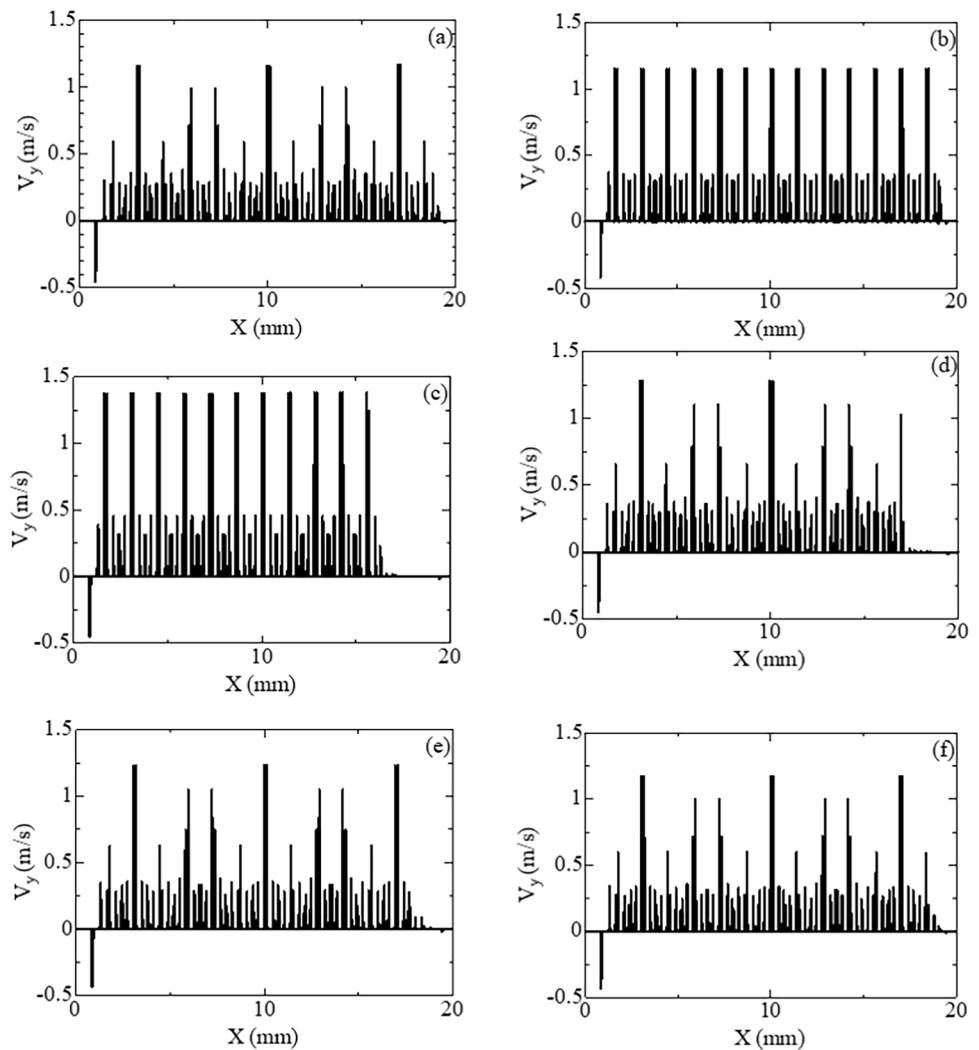


Table 2 Four contributions of initial pressure drop are shown, which are ΔP_1 at the DPF inlet, ΔP_2 across the filter wall, ΔP_3 at the DPF outlet, and ΔP_4 in the channel

Case	ΔP_1 (%)	ΔP_2 (%)	ΔP_3 (%)	ΔP_4 (%)
1	0.409	96.204	0.018	3.372
2	2.328	95.436	0.001	2.235
3	0.357	86.117	0.011	13.515
4	0.077	89.421	0.002	10.500
5	0.538	93.526	0.001	5.935
6	1.554	97.956	0.001	0.489

DPF inlet (ΔP_1), the averaged pressure drop across the DPF wall (ΔP_2), the pressure drop at the DPF outlet (ΔP_3), and the pressure drop in upper and lower channels due to the friction loss (ΔP_4) [51]. The results are shown in Table 2. Surprisingly, for all cases, the value of ΔP_2 is much larger, accounting for more than 86% of the total pressure drop. In comparison with the pressure drop across the filter wall,

the pressure drop in the channel is small, but it is relatively larger when the plug ash exists.

In our previous three-dimensional DPF simulation of the soot filtration [6, 37, 39–44], we only considered a small part of the DPF wall, because the area of the DPF wall scanned by the X-ray CT was limited. Fortunately, as shown in Table 2, most of the pressure change is observed when the exhaust gas passes through the DPF wall, even though the different ash layer distribution is given. In the case of the DPF filtration [4, 15, 16], it is well-known that the soot in the exhaust gas is firstly deposited inside the DPF wall, called the depth filtration (or the deep-bed filtration), and then, the soot deposited on the surface of the DPF wall where the pores on the filter surface are blocked with soot, called the surface filtration. In either case, the deposited soot would increase the pressure drop across the DPF wall. Therefore, for predicting the filtration process, the numerical simulation with the small part of the DPF wall can give us useful information for discussing the pressure drop.

3.2 Soot Deposition Affected by Ash Layer

Next, the soot deposition simulation was performed to investigate the effect of ash on the flow and the pressure drop. First, the result of case 1 without ash layer is described. Figure 9 shows the distributions of the soot deposition at different times. To observe the soot deposition region in detail, an enlarged area of Fig. 9 indicated by dotted line

is shown in Figs. 10, 11 and 12. Here, t is the elapsed time after we flowed soot from the inlet of the numerical domain at $x=0$ mm. In these figures, the area of the red color is the soot deposition region, that of the light blue is the filter substrate. Later in Fig. 13, the ash deposition layer is shown by the area of the yellow color. As seen in Figs. 9b and 10b at $t=21$ s, the depth filtration with soot deposition inside the filter wall is observed. At $t=54$ s, soot is deposited on the

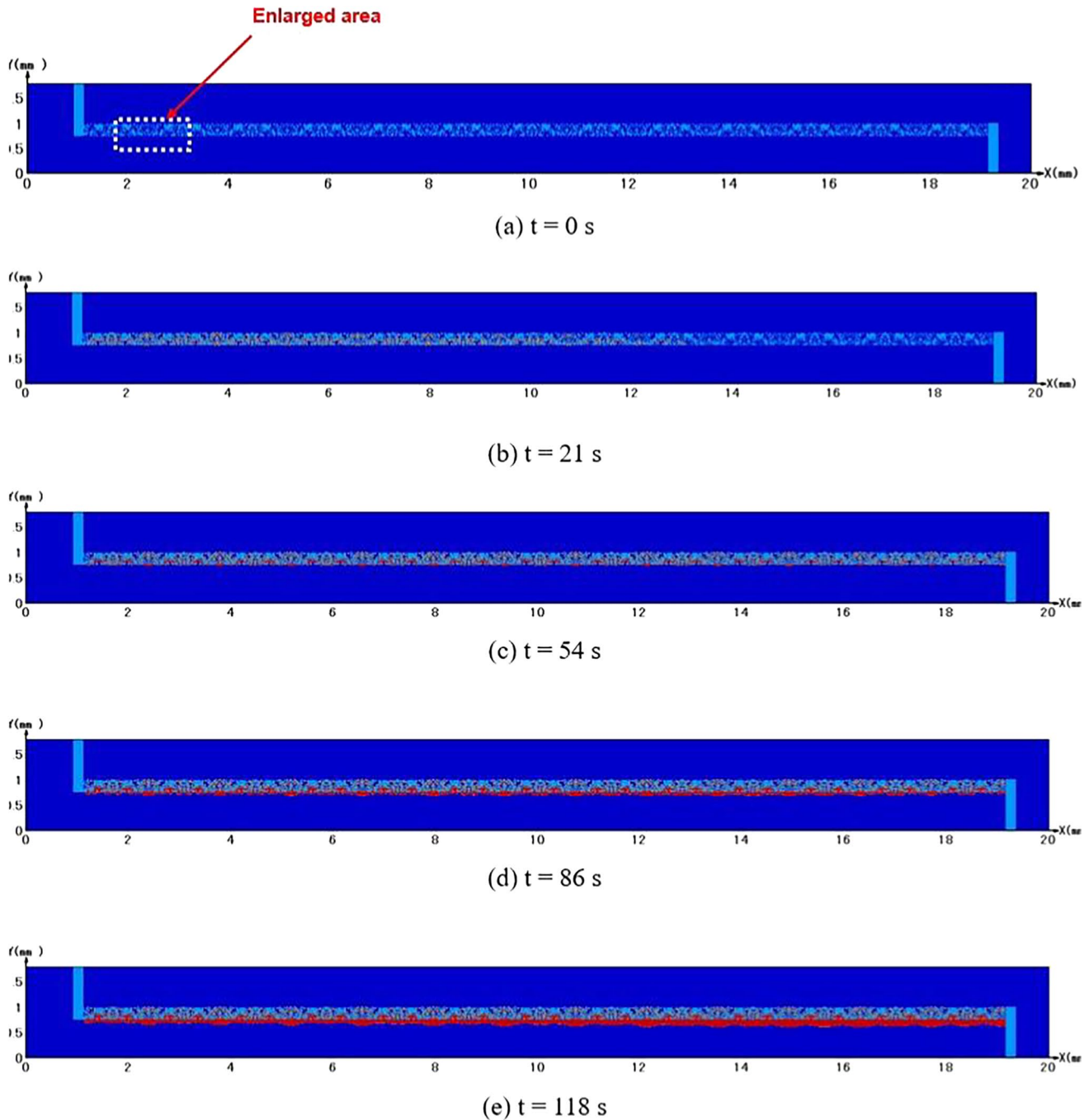


Fig. 9 Soot deposition region without ash layer in case 1

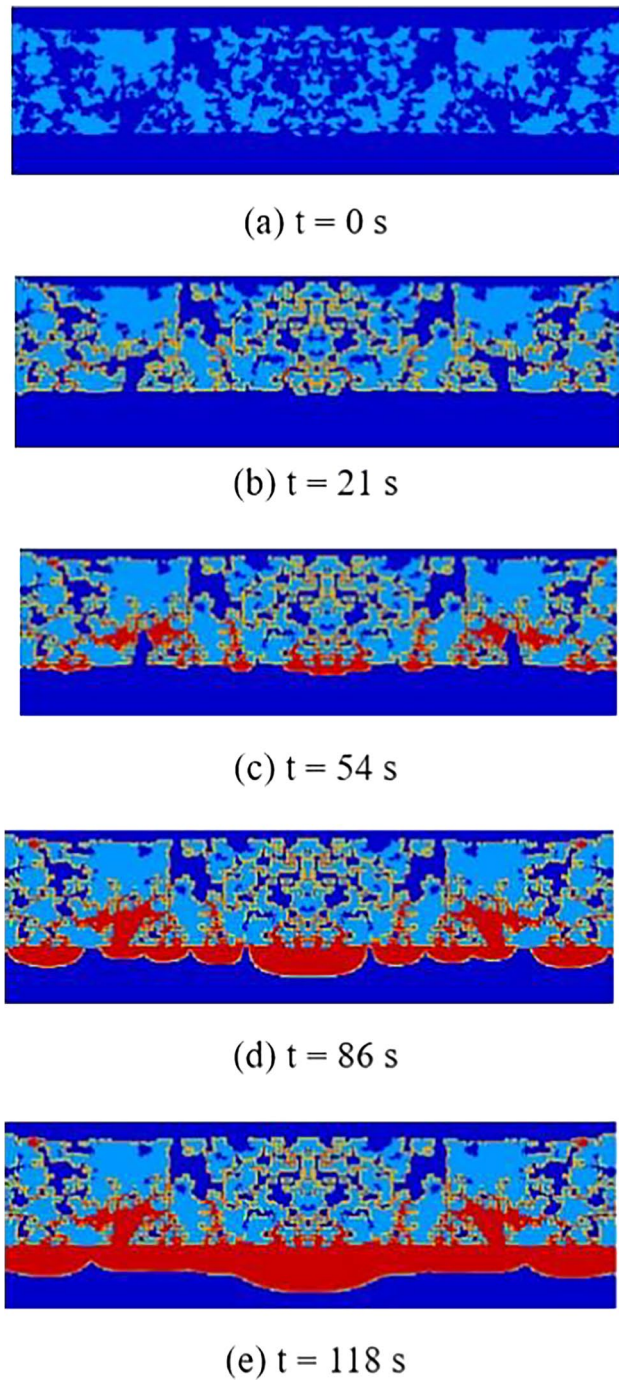


Fig. 10 Enlarged soot deposition region without ash layer in case 1

filter wall surface, in which half of the pores on the filter surface are blocked. At $t = 86$ s, all pores are blocked due to the soot deposition. At $t = 118$ s, the soot layer on the filter wall surface is thickened, indicating that the filtration process completely shifts to the surface filtration. Based on these results, the transition from the depth filtration to the surface filtration is reproduced by the two-dimensional simulation of the single channel of the DPF wall.

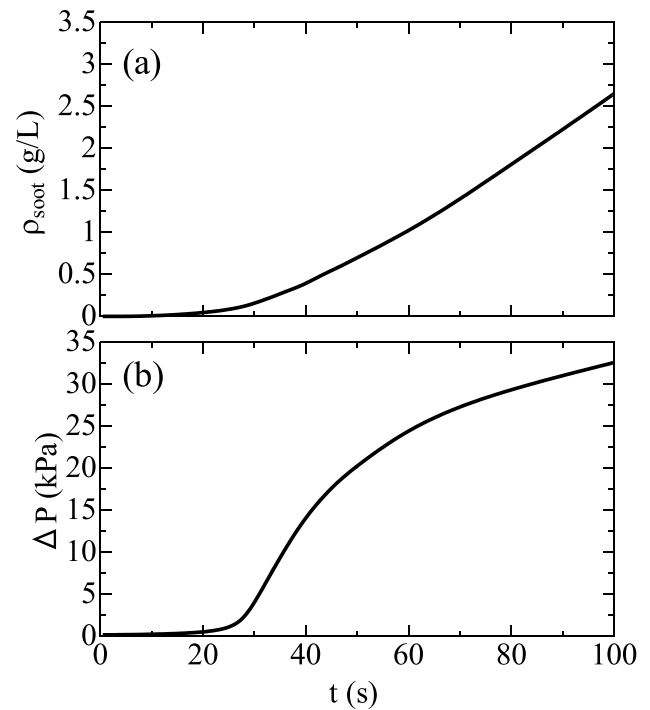


Fig. 11 Time-variations of **a** deposited soot mass and **b** pressure drop in case 1

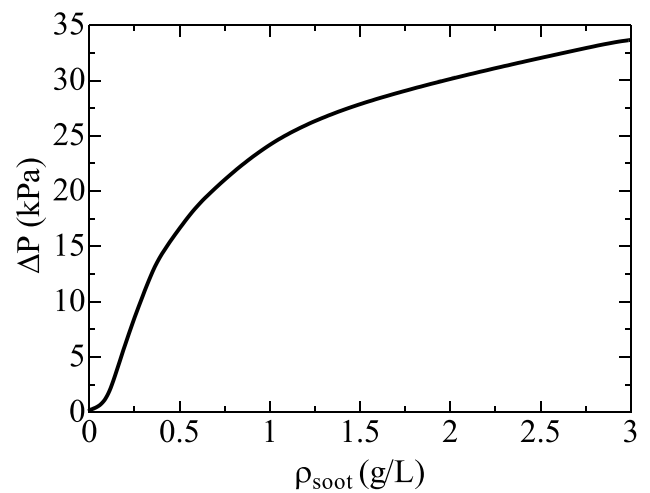


Fig. 12 Relationship between deposited soot mass and pressure drop in case 1

Figure 11 shows the time-variations of the deposited soot mass and the pressure drop in case 1, respectively. The pressure drop is the difference between pressures at the inlet and at the outlet of the DPF. It is confirmed that, at $t = 30$ to 60 s, the pressure drop increases rapidly as the amount of the soot deposition increases. However, roughly after $t = 70$ s, the increase in the pressure drop is almost linear. The same increase of the pressure drop is observed in the filter with

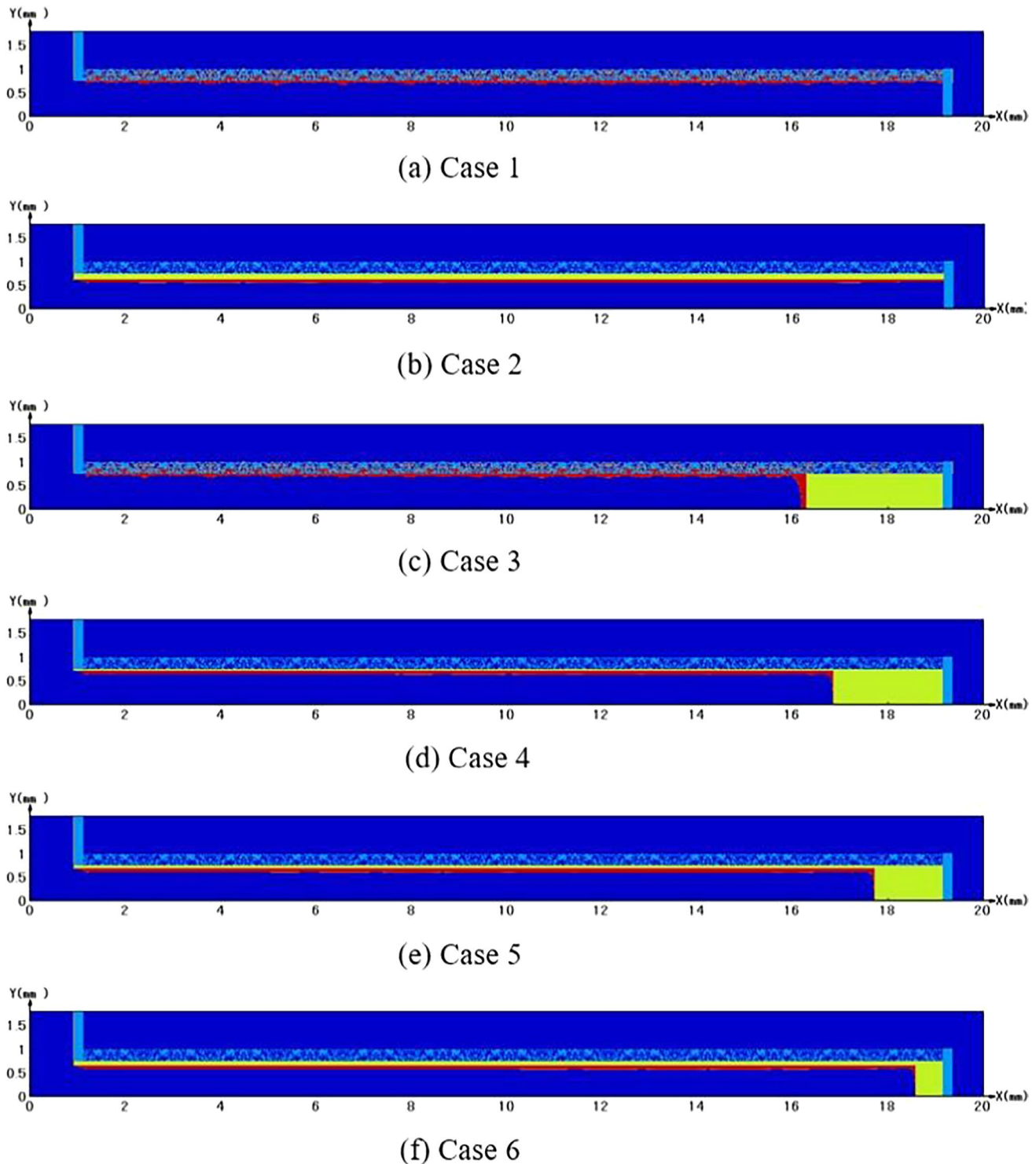


Fig. 13 Distribution of soot deposition region of $\rho_{\text{soot}} = 1.57 \text{ g/L}$ in cases 1 to 6

no ash [15, 32]. The relationship between the deposited soot mass and the pressure drop is shown in Fig. 12. The simulated pressure change is quite similar to the change in the pressure drop using the engine bench test [4, 16, 36]. It is reported that the pressure drop increases rapidly in the

depth filtration. On the other hand, in the surface filtration, the pressure drop is proportional to the amount of deposited soot, because the thickness of the soot layer increases linearly. Therefore, in this study, the relationship between the deposited soot mass and the pressure drop of the DPF

can be realized to some extent even by the two-dimensional simulation.

Next, the effects of the ash layer on the soot deposition were investigated by changing the ratio of the wall-ash and the plug-ash. Figure 13 shows the distributions of soot deposition region when the deposited soot mass is of $\rho_{\text{soot}} = 1.57 \text{ g/L}$. It is noted that these distributions in cases 1 to 6 are obtained at different times, because the time-variations of the deposited soot mass are different. Comparing Fig. 13a and b, the effect of the wall-ash on the soot deposition process can be identified. As seen in Fig. 13b, the soot deposition occurs only on the surface of the ash layer, because the soot cannot pass through the ash layer, corresponding to the “membrane effect.” It is reported that when the ash penetrates pores of the DPF wall, the depth filtration disappears and only the surface filtration occurs [25]. In the case of the plug-ash in Fig. 13c, most of the soot deposition occurs at the region without the ash, because less flow passing through the plug-ash is observed (see Fig. 7c). Since the area for the filtration is limited to the region without the plug-ash, the thickness of the soot deposition layer is larger than that in case 1. Similarly, comparing Fig. 13b with Fig. 13d–e, the soot layer on the surface of the wall-ash becomes thicker when the ratio of the plug-ash is higher.

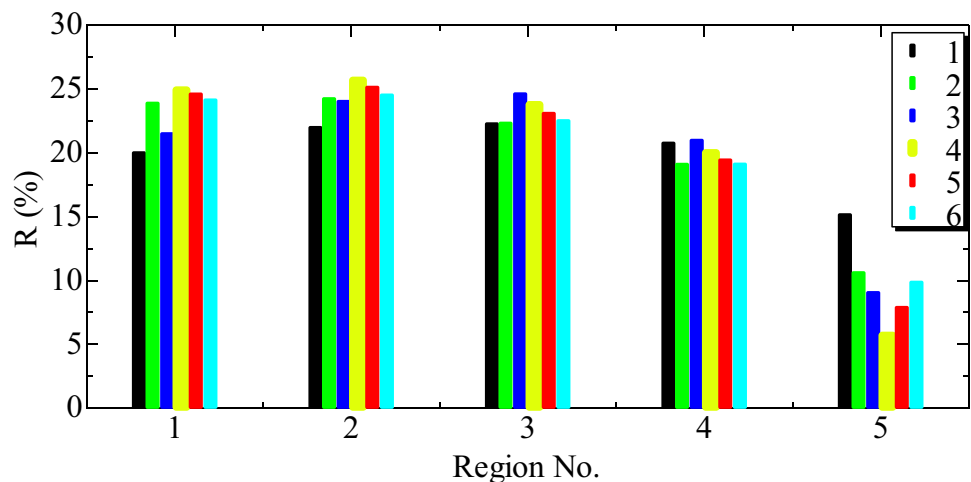
In order to examine quantitatively the effect of the ash layer distribution in Fig. 13, the soot deposition region was divided into five sections with the same width of the filter wall. From the upstream section of the filter inlet, we named regions 1 to 5. Since the filter wall is placed at $1 \text{ mm} < x < 19 \text{ mm}$, there are the region 1 at $1 \text{ mm} < x < 4.6 \text{ mm}$, the region 2 at $4.6 \text{ mm} < x < 8.2 \text{ mm}$, the region 3 at $8.2 \text{ mm} < x < 11.8 \text{ mm}$, the region 4 at $11.8 \text{ mm} < x < 15.4 \text{ mm}$, and the region 5 at $15.4 \text{ mm} < x < 19 \text{ mm}$, respectively. To see the different profiles of the deposited soot, the ratio of the soot mass deposited in each region to the total amount of deposited soot was

defined as R . The results are shown in Fig. 14. Needless to say, in cases 1 to 6, the ash amount of each region is different. From the results, it is found that more soot is deposited mostly in the upstream or the middle of the DPF, while less soot is deposited in the downstream of the DPF even in the case of no ash or wall-ash only. That is, the amount of soot deposited in the back of the DPF is relatively smaller. This tendency is different from the uniform distribution of deposited soot along the filter wall which was predicted by the one-dimensional steady flow simulation [34]. Comparing cases 1 and 3, it is found that the amount of the deposited soot in the region without the plug-ash is larger, resulting in the thicker soot layer. Comparing cases 4 to 6, it is found that, except for region 5 covered with the plug-ash, more soot is deposited in regions 1 to 4.

Figure 15 shows the time-variations of the deposited soot mass and the pressure drop in cases 1 to 6. It can be seen that the amount of the deposited soot is almost the same except for case 3. However, each pressure drop shows different tendency. The pressure drop is slightly larger as the ratio of the plug-ash increases, probably because the effective filtration area is reduced by the plug-ash. On the other hand, the pressure drops in cases 1 and 3 are much larger than those in other 4 cases. That is, the increase of the pressure drop with the wall-ash is much lower, because the ash layer prevents the depth filtration [30]. Only in cases 1 and 3, the depth filtration is observed, which would make the pressure rise steeper [15, 37]. Additionally, the value of the deposited soot mass in case 3 is larger, because the flow with soot is changed due to the plug-ash. Therefore, due to the reduced filtration area, the plug-ash could affect the amount of deposited soot as well as the pressure drop.

For further discussion on the effects of the plug-ash and the wall-ash, the relationship between the deposited soot mass and the pressure drop was investigated. The results are shown in Fig. 16. By comparing profiles in cases 1 and

Fig. 14 Fraction of deposited soot at 5 regions for cases 1 to 6



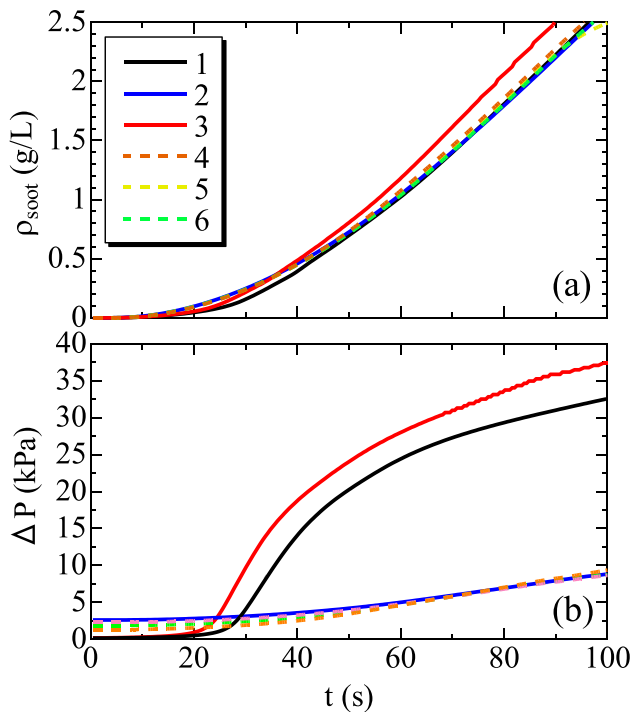


Fig. 15 Time-variations of deposited soot mass and pressure drop in cases 1 to 6

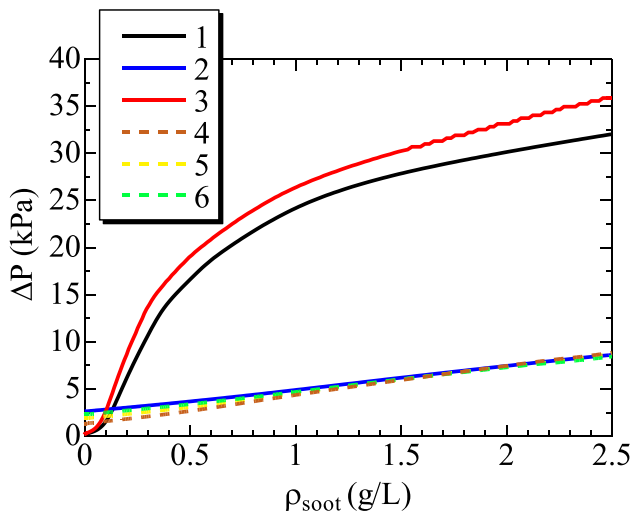


Fig. 16 Relationship between deposited soot mass and pressure drop in cases 1 to 6

3, the pressure drop in case 3 is unexpectedly larger even at the same amount of the deposited soot. Also, by comparing profiles in 1 and other four cases 2, 4–6, it is derived that the wall-ash has an opposite effect on the reduction in pressure drop. In cases 2 and 4–6, the wall-ash fully covers the surface of the DPF wall. Hence, the wall-ash can avoid the depth filtration which causes the steep pressure rise. It

is also found that the pressure drop is larger as the ratio of the wall-ash is higher. In summary, the wall-ash largely reduces the pressure drop by avoiding the depth filtration, but the thicker wall-ash layer increases the pressure drop on the condition that the total amount of the wall-ash and the plug-ash is the same.

4 Conclusions

In this study, a single channel of the DPF was simulated using a small part of the substrate structure obtained by the X-ray CT measurement. To examine the effect of the ash layer on the flow and the soot deposition, the different ash layer distributions with the wall-ash and the plug-ash were used, on the condition that the total amount of the ash was the same. As a result, the following conclusions were derived.

1. To reduce the computational costs, the different spatial grid size was tested. By comparing the steady flow, the initial pressure drop converges to a constant value when the grid size is $4 \mu\text{m}$ or smaller. Then, we simulated the soot deposition with the combination of 4 and $40 \mu\text{m}$ spatial grids. When the initial pressure drop before the soot deposition is divided into four contributions at the DPF inlet, across the filter wall, at the DPF outlet and in the channel due to the friction loss, the pressure drop across the filter wall is the largest, accounting for more than 86% of the total pressure drop. In comparison with the pressure drop across the filter wall, the pressure drop in the channel is small, but it is relatively larger when the plug ash exists. Since the value of the initial pressure drop increases at higher ratio of the wall-ash, the wall-ash has the larger effect than that of the plug-ash.
2. In the case of no ash or plug-ash only, the transition of the depth filtration to the surface filtration is observed. During the depth filtration, the pressure drop increases largely. However, when the DPF wall is fully covered with the ash, soot is deposited on the surface of the ash layer, and only the surface filtration occurs, which suppresses the increase in the pressure drop associated with the depth filtration. Comparing the case without ash, the plug-ash also increases the pressure drop, because it reduces the effective filtration area. Overall, the wall-ash largely reduces the pressure drop by avoiding the depth filtration, but the thicker wall-ash layer increases the pressure drop on the condition that the total amount of the wall-ash and the plug-ash is the same.

Acknowledgements A part of this work was supported by Isuzu Motors Ltd. in Japan.

Declarations

Conflict of Interest The authors declare that they have no competing interests.

References

- Schejbal, M., Šteřpánek, J., Marek, M., Kocří, P., Kubíček, M.: Modelling of soot oxidation by NO₂ in various types of diesel particulate filters. *Fuel* **89**, 2365–2375 (2010)
- Tsuneyoshi, K., Takagi, O., Yamamoto, K.: Effects of washcoat on initial PM filtration efficiency and pressure drop in SiC DPF, SAE Technical Paper 2011–01–0817 (2010)
- Lapuerta, M., Oliva, F., Agudelo, J.R., Boehman, A.L.: Effect of fuel on the soot nanostructure and consequences on loading and regeneration of diesel particulate filters. *Combust Flame* **159**, 844–853 (2012)
- Tsuneyoshi, K., Yamamoto, K.: Experimental study of hexagonal and square diesel particulate filters under controlled and uncontrolled catalyzed regeneration. *Energy* **60**, 325–332 (2013)
- Johnson, T.V.: Vehicular emissions in review. *SAE Int. J. Engines* **9**, 1258–1275 (2016)
- Kong, H., Yamamoto, K.: Simulation on soot deposition in in-wall and on-wall catalyzed diesel particulate filters. *Catal. Today* **332**, 89–93 (2019)
- Yamamoto, K., Yoshizawa, K.: Fuel supply system to DOC by nanopore-ceramic tube and measurement of fuel evaporation rate. *Fuel* **298**(14) (2021)
- Ximinis, J., Massaguer, A., Pujol, T., Massaguer, E.: NO_x emissions reduction analysis in a diesel Euro VI Heavy Duty vehicle using a thermoelectric generator and an exhaust heater. *Fuel* **301** (2021)
- Gong, J., Viswanathan, S., Rothamer, S.A., Foster, D.A., Rutland, C.J.: Dynamic heterogeneous multiscale filtration model: probing microand macroscopic filtration characteristics of gasoline particulate filters. *Environ. Sci. Technol.* **51**, 11196–11204 (2017)
- Czerwinski, J., Comte, P., Heeb, N., Mayer, A., Hensel, V.: Nanoparticle emissions of DI gasoline cars with/without GPF, SAE Technical Paper 2017–01–1004, 1–8 (2017)
- Jang, J., Lee, J., Choi, Y., Park, S.: Reduction of particle emissions from gasoline vehicles with direct fuel injection systems using a gasoline particulate filter. *Sci. Total Environ.* **644**, 28–33 (2018)
- Yamamoto, K., Kondo, S., Suzuki, K.: Filtration and regeneration performances of SiC fiber potentially applied to gasoline particulates. *Fuel* **243**, 28–33 (2019)
- Chen, L., Liang, Z., Zhang, X., Shuai, S.: Characterizing particulate matter emissions from GDI and PFI vehicles under transient and cold start conditions. *Fuel* **189**, 131–140 (2017)
- Adler, J.: Ceramic diesel particulate filters. *Int. J. Appl. Ceramic Tech.* **2**, 429–439 (2005)
- Wirojsakunchai, E., Schroeder, E., Kolodziej, C., Foster, D.E., Schmidt, N., Root, T., Kawai, T., Suga, T., Nevius, T., Kusaka, T.: Detailed diesel exhaust particulate characterization and real-time DPF filtration efficiency measurements during PM filling process, SAE Technical Paper 2007–01–0320 (2007)
- Beatrice, C., Iorio, S.D., Guido, C., Napolitano, P.: Detailed characterization of particulate emissions of an automotive catalyzed DPF using actual regeneration strategies. *Exp. Ther. Fluid Sci.* **39**, 45–53 (2012)
- Tsuneyoshi, K., Yamamoto, K.: A Study on the cell structure and the performances of wall-flow diesel particulate filter. *Energy* **48**, 492–499 (2012)
- Gülmez, Y., Özmen, G.: Effects of exhaust backpressure increment on the performance and exhaust emissions of a single cylinder diesel engine. *J. ETA Maritime Sci.* **9**(3), 177–191 (2021)
- Warner, J.R., Dobson, D., Cavataio, G.: A study of active and passive regeneration using laboratory generated soot on a variety of SiC diesel particulate filter formulations. *SAE Int J Fuels Lubricants* **3**(1), 149–164 (2010)
- Chen, C., Yao, A., Yao, C., Qu, G.: Experimental study of the active and passive regeneration procedures of a diesel particulate filter in a diesel methanol dual fuel engine, *Fuel* **264** (2020)
- R’Mili, B., Boréave, A., Meme, A., Vernoux, P., Leblanc, M., Noël, L.: Physico-chemical characterization of fine and ultrafine particles emitted during diesel particulate filter active regeneration of Euro5 diesel vehicles. *Environ. Sci. Technol.* **52**(5), 3312–3319 (2018)
- Suresh, A., Yezerets, A., Currier, N., Clerc, J.: Diesel particulate filter system—effect of critical variables on the regeneration strategy development and optimization. *SAE Int. J. Fuels and Lubricants* **1**(1), 173–183 (2009)
- Yamamoto, K., Kato, H., Suzuki, D.: Pressure response during filtration and oxidation in diesel particulate filter. *Emission Control Sci. Tech.* **5**(1), 24–30 (2019)
- Li, Z., Li, S., Li, Z., Wang, Y., Li, Z., Li, M., Jiao, P., Cai, D.: Simulation study of NO₂-assisted regeneration performance of variable cell geometry catalyzed diesel particulate filter. *Process Saf. Environ. Prot.* **154**, 211–222 (2021)
- Zhang, J., Li, Y., Wong, V.W., Shuai, S., Qi, J., Wang, G., Liu, F., Hua, L.: Experimental study of lubricant-derived ash effects on diesel particulate filter performance. *Int. J. Engine. Res.* **22**(3), 921–934 (2021)
- Aravelli, K., Heibel, A.: Improved lifetime pressure drop management for robust cordierite (RC) filters with asymmetric cell technology (ACT), SAE Paper 2007–01–0920 (2007)
- Sappok, A., Santiago, M., Vianna, T. and Wong, W.V.: Characteristic and effects of ash accumulation on diesel particulate filter performance: rapidly aged and filed aged results, SAE Paper 2009–01–1086 (2009)
- Sappok, A., Rodriguez, R., Wong, V.: Characteristic and effects of lubricant additive chemistry on ash properties impacting diesel particulate filter service life, SAE Paper 2010–01–1213 (2010)
- Ishizawa, T., Yamane, H., Satoh, H., Sekiguchi, K.: Investigation into ash loading and its relationship to DPF regeneration method, SAE Paper, 2009–01–2882 (2009)
- Jiang, J., Gong, J., Liu, W., Chen, T., Zhong, C.: Analysis on filtration characteristic of wall-flow filter for ash deposition in cake. *J. Aerosol Sci.* **95**, 73–83 (2016)
- Fang, J., Meng, Z., Li, J., Pu, Y., Du, Y., Li, J., Jin, Z., Chen, C., Chase, G.G.: The influence of ash on soot deposition and regeneration processes in diesel particulate filter. *Appl. Thermal. Eng.* **124**, 633–640 (2017)
- Lao, C.T., Akroyd, J., Smith, A., Morgan, N., Lee, K.F., Nurkowski, D., Kraft, M.: Modelling investigation of the thermal treatment of ash-contaminated particulate filters. *Emiss. Control Sci. Technol.* **7**, 265–286 (2021)
- Konstandopoulos, A.G., Kostoglou, M., Skaperdas, E., Papaioannou, E.: Fundamental studies of diesel particulate filters: transient loading, regeneration and aging, SAE Technical paper 2000–01–1016 (2000)
- Koltsakis, G., Haralampous, O., Depcik, C., Ragone, J.C.: Catalyzed diesel particulate filter modeling. *Rev. Chem. Eng.* **29**(1), 1–61 (2013)
- Wang, Y., Wong, V., Sappok, A., Munnis, S.: The sensitivity of DPF performance to the spatial distribution of ash inside DPF inlet channels, SAE Technical paper 2013–01–1584 (2013)

36. Uenishi, T., Tanaka, T., Shigeno, G., Fukuma, T., Kusaka, J., Daisho, Y.: A quasi two dimensional model of transport phenomena in diesel particulate filters—the effects of particle and wall pore diameter on the pressure drop, SAE Paper 2015–01–2010 (2015)
37. Yamamoto, K., Tajima, Y.: Mechanism for pressure drop variation caused by filtration of diesel particulates. *Int. J. Engine. Res.* **22**, 632–639 (2019). <https://doi.org/10.1177/1468087419853738>
38. Sappok, A., Wong, V.: Ash effects on diesel particulate filter pressure drop sensitivity to soot and implications for regeneration frequency and DPF control, SAE Technical paper 2010–01–0811 (2010)
39. Yamamoto, K., Satake, S., Yamashita, H., Takada, N., Misawa, M.: Lattice Boltzmann simulation on porous structure and soot accumulation. *Math. Comp. Sim.* **72**, 257–263 (2006)
40. Yamamoto, K., Nakamura, M.: Simulation on flow and heat transfer in diesel particulate filter, *ASME J. Heat Transfer* **133**(6) (2011). <https://doi.org/10.1115/1.4003448>
41. Yamamoto, K., Yamauchi, K.: Numerical simulation of continuously regenerating diesel particulate filter. *Proc. Combust. Inst.* **34**, 3083–3090 (2013)
42. Yamamoto, K., Ohori, S.: Simulation on flow and soot deposition in diesel particulate filter. *Int. J. Engine. Res.* **14**, 333–340 (2013)
43. Yamamoto, K., Sakai, T.: Simulation of continuously regenerating trap with catalyzed DPF. *Catal. Today* **242**, 357–362 (2015)
44. Yamamoto, K., Yagasaki, S.: Numerical simulation of particle-laden flow and soot layer formation in porous filter. *Solids* **3**, 282–294 (2022)
45. Chen, S., Doolen, G.D.: Lattice Boltzmann method for fluid flows. *Annu. Rev. Fluid. Mech.* **30**, 329–364 (1998)
46. Qian, Y.H., D’Humières, D., Lallemand, P.: Lattice BGK models for Navier-Stokes equation. *Eur. Lett.* **17**, 479–484 (1992)
47. Filippova, O., Succi, S., Mazzocco, F., Arrighetti, C., Bella, G., Hanel, D.: Multiscale lattice Boltzmann schemes with turbulence modeling. *J. Comp. Phys.* **170**, 812–829 (2001)
48. Konstandopoulos, A.G., Skaperdas, E.: Microstructural properties of soot deposits in diesel particulate traps, SAE Technical paper 2002–01–1015 (2002)
49. Wang, Y., Kamp, C.J., Wang, Y., Toops, T.J., Su, C., Wang, R., Gong, J., Wong, V.W.: The origin, transport, and evolution of ash in engine particulate filters. *Appl. Energy* **263**(1), 114631 (2020)
50. Konstandopoulos, A.G.: Flow resistance descriptors for diesel particulate filters: definitions, measurements and testing, SAE Technical paper 2003–01–0846 (2003)
51. Wang, Y., Wong, V., Sappok, A., Rodriguez, R. and Munnis, S.: The sensitivity of DPF performance to the spatial distribution of ash inside DPF inlet channels, SAE Paper 2013–01–1584 (2013)

Publisher's Note Springer Nature remains neutral with regard to jurisdictional claims in published maps and institutional affiliations.

Springer Nature or its licensor holds exclusive rights to this article under a publishing agreement with the author(s) or other rightsholder(s); author self-archiving of the accepted manuscript version of this article is solely governed by the terms of such publishing agreement and applicable law.